Korean J. Chem. Eng., 35(12), 2430-2441 (2018)
DOI: 10.1007/s11814-018-0155-0

pISSN: 0256-1115
eISSN: 1975-7220

Synthesis of binary Cu-Se and In-Se nanoparticle inks using cherry blossom gum for $CuInSe_2$ thin film solar cell applications

Babu Pejjai*,*, Vasudeva Reddy Minnam Reddy*, Kondaiah Seku**, Haeyun Cho*, Mohan Reddy Pallavolu*, Trang Thi Thuy Le*, Dong-seob Jeong*, Tulasi Ramakrishna Reddy Kotte***, and Chinho Park*,†**

*School of Chemical Engineering, Yeungnam University, 280 Daehak-ro, Gyeongsan 38541, Korea
**Department of Chemistry, Shinas College of Technology, Shinas, Sultanate of Oman
***Solar Energy Laboratory, Department of Physics, Sri Venkateswara University, Tirupati 517502, India
(*Received 11 April 2018 • accepted 22 September 2018*)

Abstract−Selenium (Se)-rich binary Cu-Se and In-Se nanoparticles (NPs) were synthesized by a modified heat-up method at low temperature (110 °C) using the gum exudates from a cherry blossom tree. Coating of CISe absorber layer was carried out using Se-rich binary Cu-Se and In-Se NPs ink without the use of any external binder. Our results indicated that the gum used in the synthesis played beneficial roles such as reducing and capping agent. In addition, the gum also served as a natural binder in the coating of CISe absorber layer. The CISe absorber layer was integrated into the solar cell, which showed a power conversion efficiency (PCE) of 0.37%. The possible reasons for low PCE of the present solar cells and the steps needed for further improvement of PCE were discussed. Although the obtained PCE is low, the present strategy opens a new path for the fabrication of eco-friendly CISe NPs solar cell by a relatively chief non-vacuum method.

Keywords: Cherry Blossom Tree Gum Assisted Synthesis, Binary Cu-Se and In-Se NPs, Non-vacuum Air-spray Coating, CISe NPs Solar Cell

INTRODUCTION

In view of the limited availability of fossil fuels and growing environmental problems, there is a strong demand for the production of renewable energies at lower prices. Renewable energy sources such as biomass, wind, solar, geothermal, and biodiesel are proposed as alternatives to fossil fuels [1,2]. Among these, solar energy is considered to be one of the most promising as it is clean and abundant. Many advances have been reported in this sector starting from the traditional crystalline silicon solar cells to CdTe technology. Even though the crystalline silicon and CdTe solar cells showed record efficiency, an extensive use of these solar cells is limited due to high cost crystalline silicon and toxicity (CdTe) solar cells. Alternatively, a thin film solar cell based on $CuInSe_2$ (CISe) has been proposed. CISe, one of the most promising absorber materials in ternary semiconductors, has been widely used in the field of thin film photovoltaic devices (PVs) [3]. It has a high absorption coefficient of 10^5 cm^{-1} and its band gap energy can be modulated between 1.05 eV and 1.68 eV by the partial substitution of indium with gallium [4,5]. The first thin-film $CuInSe_2$/CdS devices were fabricated by Kazmerski et al. [6] through the evaporation of $CuInSe_2$ powder in the Se-rich environment. Recently, a power conversion efficiency (PCE) of 22.6% was reported for $Cu(In,Ga)Se_2$ (CIGSe) based solar cell prepared by vacuum deposition methods [7]. Although the vacuum deposited CISe or CIGSe solar cells showed high conversion efficiency, their fabrication required a large capitalization due to the requirement of high vacuum and temperatures. The high vacuum and high-temperature requirements eventually lead to high production cost as well as limitations in the device architecture of these solar cells. Alternatively, a significant cost reduction with amicable device architecture can be produced when processed by an inexpensive high throughput non-vacuum methods [8-12].

In this direction, numerous reports with different strategies were also published on the synthesis as well as on the fabrication of CISe or CIGSe nanoparticles (NPs) solar cells [8-10,13-21]. Among the reported strategies [8-10,13-21], the preparation of CISe or CIGSe absorber layers using binary or multiphase nanoparticles route is unique for the following reasons: (1) If fine crystalline particles are used to obtain the CISe/CIGSe absorber layers, they require high processing temperatures during a post-thermal treatment owing to the sharp melting point [15]. Eventually, the production cost of the solar cell is again increased due to the requirement of the high thermal budget. Instead, if amorphous or binary NPs are used to obtain the CISe/CIGSe absorber layers, they can be easily processed even at lower temperatures [15,22]. Therefore, the production cost of the solar cell can be reduced; (2) the grading of band gap energy is also easy in the case of binary NPs blended CISe/CIGSe absorber layer owing to the precise controllability ride over the composition of binary NPs [23]; (3) often the anions were lost as byproducts in the synthesis of CISe by the metal salt precursors, but the loss of these anions is also avoided when binary metal selenides are used as the precursors [15]. Therefore, the use of binary metal selenide NPs is more favorable in the deposition of CIGSe/CISe NPs absorber layers.

On the other hand, the solvents used in the synthesis of CISe/

†To whom correspondence should be addressed.
E-mail: chpark@ynu.ac.kr

CIGSe NPs also play an important role in determining the environmental and health concerns as well as the production cost of the CISe/CIGSe solar cells. For example, solvents such as trioctylphosphine, trioctylphosphine oxide, tributylphosphine, diphenylphosphine, and hydrazine have high toxicity, whereas the solvents (with a high boiling point) such as oleylamine and octadecene need high synthesis temperatures (>200 °C) [24-26]. In this scenario, the synthesis of binary or ternary Cu-In-Se NPs using plant extracts is safer and economical. The plant extracts can act as both reducing and stabilizing agents [27]. In addition, it is very chief, abundant, and non-toxic. Often, the plant exudates such as gum karaya, gum arabic have been used as both reducing and stabilizing agents in the synthesis of metal nanoparticles such as gold, silver, and copper [27-30]. Gums are polysaccharides which contain functional groups such as CH_3, C=C, C-O, and C-N [31]. These functional groups in the gum are responsible for the action of reducing and stabilizing agent effects.

Therefore, our intent here is to describe the coating of CISe absorber layer from the binary Cu-Se and In-Se NPs. The binary (Cu-Se and In-Se) NPs were synthesized by a modified heat-up method at low temperature (110 °C) using a gum (NG) exudate from the cherry blossom tree. To the best of our knowledge, no CISe thin film solar cells have been reported so far using the cherry blossom tree gum assisted binary Cu-Se and In-Se NPs. The present approach eliminates the need for any air-sensitive, toxic, and expensive starting materials. Further, it is observed that the use of NG not only acts as reducing/capping agent in the synthesis of binary (Cu-Se and In-Se) NPs, but it also provides the necessary viscosity to the ink (which is highly desirable to adjust the paste rheology) [32].

Many works have been published on ink-based CIS cells [8-10, 13-21]. Most of the investigators have used external organic binders such as ethyl cellulose, polyvinylpyrrolidone, and Terpineol etc. to prepare the nanoparticle inks [33]. Even though the addition of external organic binders prevents the delamination and microcracking of the film in the post-annealing steps [34], the added binders may leave a thick layer of carbon near to Mo-back contact [34-36]. The formation of thick carbon layer usually shows a detrimental effect on the power conversion efficiency of CISe NPs solar cells. One possible solution to this problem is the use of NG. NG can act as both reducing/capping agent in the synthesis of binary NPs as well as the internal binder in the ink preparation as it provides the necessary viscosity to ink.

Therefore, in the present method, the Cu-In-Se precursor films were coated on bare soda lime glass (SLG) and molybdenum SLG substrates without the use of any other organic additives. It has been observed that the coated CISe films were free from any microcracks due to the desired viscosity adjustment and binder action provided by NG. Thus, the method followed herein has the following advantages: (i) the synthesis of binary NP is eco-friendly, as it involves less toxic and greener solvents such as NG; (ii) Se-rich binary NPs were used to obtain the CISe absorber layer; therefore, it alleviates the use of toxic selenization steps such as H_2Se annealing; (iii) the present method is facile and economic, as all manipulations of binary NP were carried out at low temperature under atmospheric conditions with simple equipment. Therefore, the present strategy is beneficial and reduces the production cost of the absorber material.

EXPERIMENTAL DETAILS

1. Chemicals

All chemicals were used as received. Copper (II) chloride ($CuCl_2 \cdot 2H_2O$, 99%) was purchased from Alfa Aesar. Indium (III) chloride ($InCl_3$, 99.99%) and elemental selenium (Se, 99.99%) were obtained

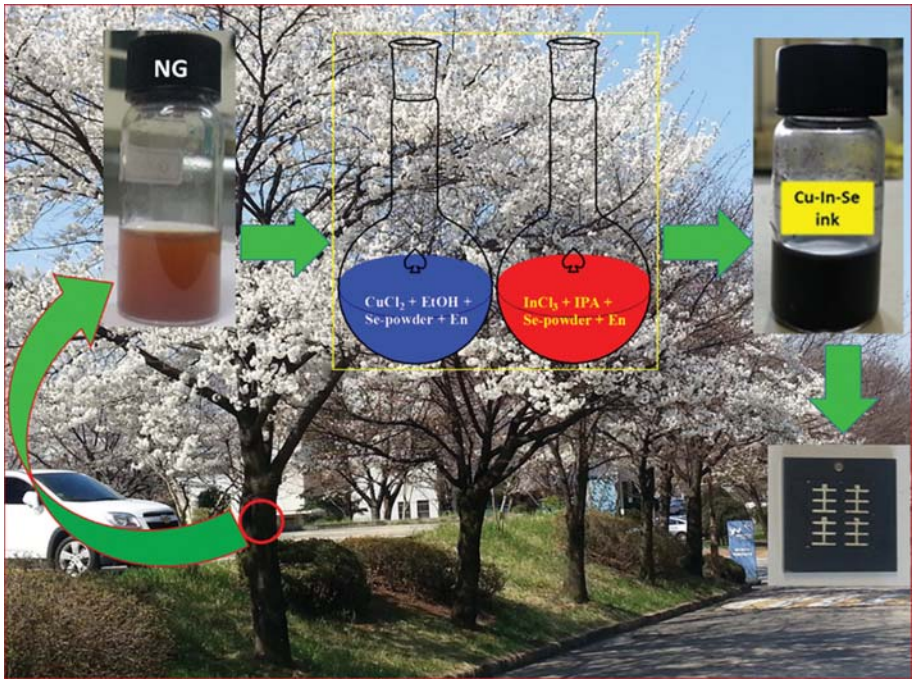

Fig. 1. Schematic of CISe solar cell fabrication using cherry blossom tree gum assisted binary Cu-Se and In-Se NPs ink.

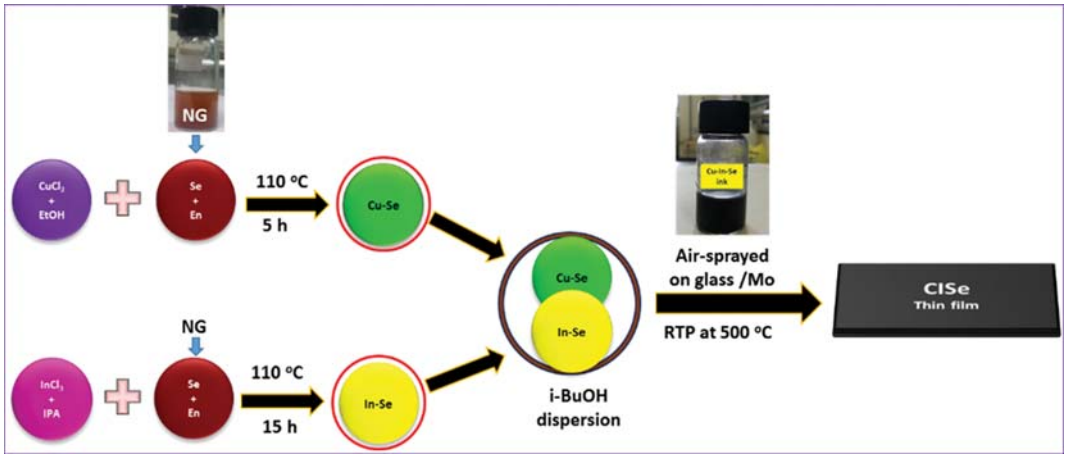

Fig. 2. Schematic of Cu-Se and In-Se NPs synthesis and CISe absorber coating.

from Sigma Aldrich. Ethylenediamine anhydrous (en, 97%) was purchased from Daejung Chemical & Metal Co., Ltd. Monoethanolamine (MEA, 99.5%), n-propyl alcohol (IPA, 99.5%), isobutyl alcohol (i-BuOH, 99%), ethyl alcohol, (EtOH, 94%) and methyl alcohol (MeOH, 99.8%) were purchased from Duksan Pure Chemicals Co., Ltd. The gum (NG, 2 g/20 ml of D.I water) used in the reaction was collected from the tree of cherry blossom on the campus of Yeungnam University and then purified. Fig. 1 shows the digital image of cherry blossom trees, purified cherry blossom gum, schematic of binary NPs synthesis, and the fabricated CISe solar cell.

2. Synthesis of Binary Cu-Se and In-Se NPs

The schematic of binary Cu-Se and In-Se NPs synthesis is illustrated in Fig. 2. As all manipulations were carried at atmospheric conditions, the present method is facile.

(i) Cu-Se NPs: First, 0.02 mol of elemental Se-powder was dissolved into 20 mL of 'en' with or without the addition of NG (see inset of Fig. 2) in a two-neck round-bottom flask and stirred vigorously at 90 °C for 1 h (a color change from black to dark-brown was observed). Meanwhile, 0.01 mol of $CuCl_2 \cdot 2H_2O$ was dissolved in 20 mL of EtOH in a reaction flask and stirred at room temperature. Then, these two solutions were mixed together with a constant stirring and allowed to react at a reaction temperature of 110 °C for 5 h. The slurry was cooled to room temperature by adding excess EtOH into the reaction mixture. A black precipitate was separated by centrifugation followed by alternative washing steps in methanol and D. I. water. Finally, the obtained NPs was dried at 80 °C under vacuum for 5 h and used for characterizations.

(ii) In-Se NPs: 0.01 mol of $InCl_3$ was dissolved in 20 ml of IPA at room temperature as the source of indium ions. This solution was mixed with elemental Se dissolved 'en' with or without the addition of NG. Synthesis of In-Se NPs was also carried out at 110 °C, but for 15 h. Yellow precipitate was obtained as the final product. Other remaining steps such as washing and drying are same as stated in the synthesis of Cu-Se NPs.

3. Preparation of CISe Absorber Layer

First, binary Cu-Se and In-Se NPs (1 : 1 w/w ratio) were dispersed in i-BuOH : MEA to form the stable ink. A digital photographic image of i-BuOH : MEA dispersed Cu-Se and In-Se NPs ink is shown in the inset of Fig. 2. Particular characteristics of i-BuOH : MEA dispersion are its low boiling point (108 °C for i-BuOH and 170 °C for MEA) and suitable viscosity (3.95 cP at 20 °C for i-BuOH and 24,100 cP for MEA) for air-spray. However, a small quantity of MeOH was also used in the film coating to adjust the ink viscosity.

Next, the soda lime glass substrates or molybdenum coated soda lime glass substrates were pre-heated to 80 °C using a hot-plate, and the ink was then air-sprayed onto the substrates. To obtain the CISe absorber layers, the precursor films were rapid thermal processed (RTP) at 500 °C for 20 min under inert atmosphere (N_2 gas) with 100 mTorr pressure.

4. Solar Cell Fabrication

To check the photovoltaic potential of the present CISe NPs, the solar cells with device architecture of SLG/Mo/CIS/CdS/i-ZnO/Al : ZnO/Ni/Ag were fabricated and tested. CdS buffer layer of thickness ~70 nm was deposited onto the CISe absorber by chemical bath deposition (CBD) technique. The details of the CdS buffer layer deposition are given in our previous report [37]. 50 nm i-ZnO and Al-doped ZnO (350 nm) layers were deposited onto the CdS layer using radio-frequency (RF) and D.C magnetron sputtering, respectively. Ni (50 nm) and Ag (500 nm) metal grids were deposited by electron beam evaporation as a top contact. The active area of each completed solar cell was 0.16 cm^2.

5. Characterizations

The crystalline structure, morphology, and composition of the binary NPs, as-deposited films, and annealed films were analyzed by X-ray diffraction (PANalyticalX'Pert-PRO MPD) using CuK_α line (λ=1.056 nm), scanning electron microscopy (SEM; Hitachi S-4800) and energy dispersive spectroscopy (EDS), respectively. To obtain in-depth information about the binary NPs, a transmission electron microscopy (TEM; 20 kV; Tecnai G2 F20 S-TWIN) observation was performed. Thermal stability of as-synthesized binary NPs and Cu-In-Se precursor film was examined by thermogravimetric-differential thermal analysis (TG-DTA) combined with simultaneous differential scanning calorimeter (DSC) (Model: SDT Q600). In the TG-DTA analysis, the samples were heated at a ramp rate of 10 °C/min under N_2 flow. To perform a TG-DTA analysis on the Cu-In-Se precursor film, the film was scrubbed from the sub-

strate, and the powder obtained was used in the TG-DTA analysis. Raman analysis was performed on CISe absorber layer at room temperature by HORIBA Raman spectrometer (Model: Xplora Plus) using 532 nm Laser as an excitation light source. The optical absorbance of CISe films was measured using a Cary 5000 UV-Vis-NIR double beam spectrophotometer in the wavelength (λ) range of 400-1,600 nm. For UV-Vis-NIR analysis, a parallel sample prepared on bare soda lime glass was used with an uncoated soda lime glass as the reference. These films were processed identically by all means as that of CISe films deposited on the Mo-coated soda lime glass substrates. The illuminated current density-voltage (J-V) characteristics of the device were measured with Keithley 2400 equipment. A Xenon flash lamp (USHIO, flash type, UA-DF1, 1,000 W, 400 V) with AM 1.5 filter was used as a source of light.

RESULTS AND DISCUSSION

1. Properties of Binary Cu-Se and In-Se NPs

1-1. Structural Analysis

Fig. 3 shows the X-ray diffraction patterns of binary Cu-Se and In-Se NPs with or without NG. Without NG, the XRD patterns of binary NPs showed peaks of hexagonal selenium, $CuSe_2$, $Cu_4O(SeO_3)_3$, InSe, In_2O_3, indium, and selenium chlorides, which indicates the partial disassociation and oxidization of the precursors [38]. However, with NG, the XRD patterns of binary NPs showed peaks of hexagonal selenium, $CuSe_2$, Cu_5Se_4, Cu_7Se_4, In_2Se_3, In_4Se_3, In_2Se_3, In_4Se_3, and chlorides of indium and selenium (JCPDS-2004). Interestingly, in the case of NG assisted binary NPs synthesis, the NPs were not oxidized due to surface passivation by NG. In addition, all the precursors were promptly disassociated and reacted to yield binary NPs with aforesaid multiple phases. The reaction between the precursors and NG was also confirmed by FTIR analysis. As mentioned in the introduction section, the Se-rich multiphase Cu-In-Se NPs route is unique owing to low budget post-heat treatment and easy controllability over the selenium losses. Therefore, in the present case also, the obtained NG assisted binary NPs with Se-rich multiphase were considered as amicable for the fabrication of CISe NPs solar cell. Therefore, the NG assisted binary NPs were further characterized in detail.

1-2. Compositional Analysis

To measure the composition of binary NPs, EDS analysis was carried out on the samples. Fig. 4 shows the EDS spectra of binary Cu-Se and In-Se NPs with or without NG. The EDS spectrum of binary NPs (both Cu-Se and In-Se) synthesized without NG showed peaks of O, Cl, Cu, In, Se, with a little amount of carbon. In contrast, the EDS spectrum of NG assisted binary NPs showed peaks of Cl, Cu, In, and Se with a little amount of carbon. In the case of NG assisted binary NPs, the peaks related to oxygen were not identified, at least within the detection limit of EDS (the uncertainty of EDS analysis is ±2 at%). Further, a relatively high-intensity peak corresponding to 'Se' in the EDS spectra of both NPs indicates the Se-rich composition of binary NPs.

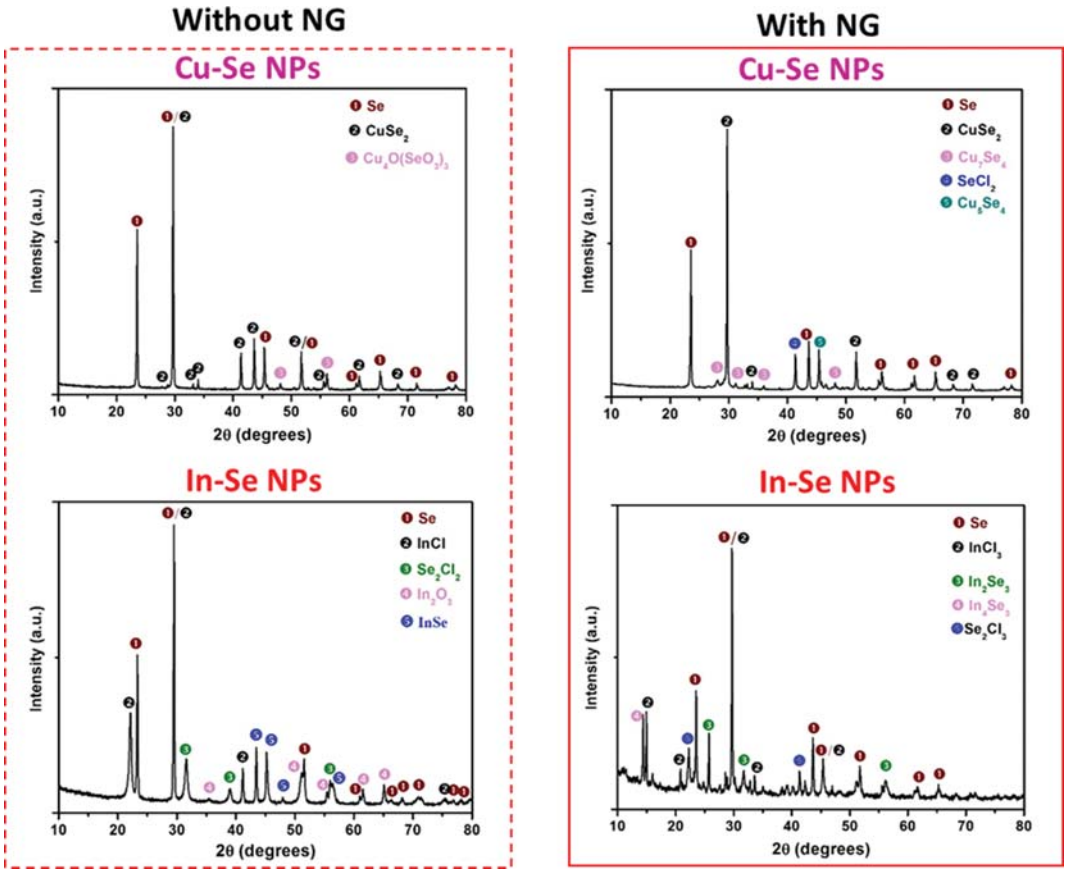

Fig. 3. XRD patterns of binary Cu-Se and In-Se nanoparticles.

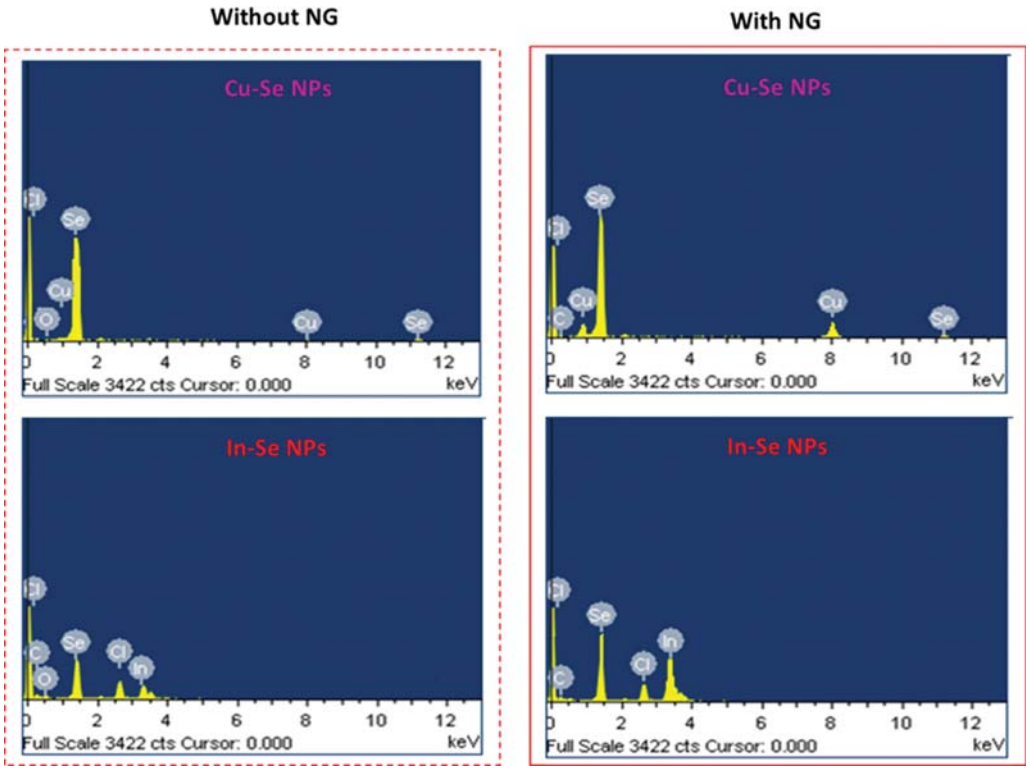

Fig. 4. EDS spectra of binary Cu-Se and In-Se nanoparticles.

From the EDS analysis, it is clear that the presence of NG prevents the oxidation of metal ions as it passivates the surface of NPs. Similarly, the XRD results also confirmed the formation of Se-rich binary NPs without oxidation in the case of NG assisted synthesis. Therefore, the use of NG is beneficial as the surface capping and reducing agent in the synthesis of binary NPs. The growth rate of NPs depends on the factors such as the steric size of the ligand molecule, the bond strength between the metallic monomers, and ligand molecule [39]. Consequently, the binary NPs in the presence of NG were grown in a controlled environment with different morphologies. For this reason, further studies were carried out only on the NG assisted binary NPs.

1-3. Morphological Analysis

Fig. 5(a0)-(b2) shows the morphology of NG assisted binary NPs examined by SEM. The Cu-Se NPs show hexagonal and cylindrical rods. The size of Cu-Se NPs was in the range of 0.5-1.4 μm with a thickness of 30-100 nm. The growth of large hexagonal shapes of Cu-Se NPs is due to the presence of $CuSe_2$/CuSe phase, which assists the liquid phase growth [40]. The SEM images of In-Se NPs show irregular shape flakes of ~20-80 nm thick. A magnified view of the SEM images indicates the smooth and finished surface to Cu-Se NPs (Fig. 5(a1)-(a2)), whereas the surface of In-Se NPs decorated with small and irregular shaped particles (Fig. 5(b1)-(b2)).

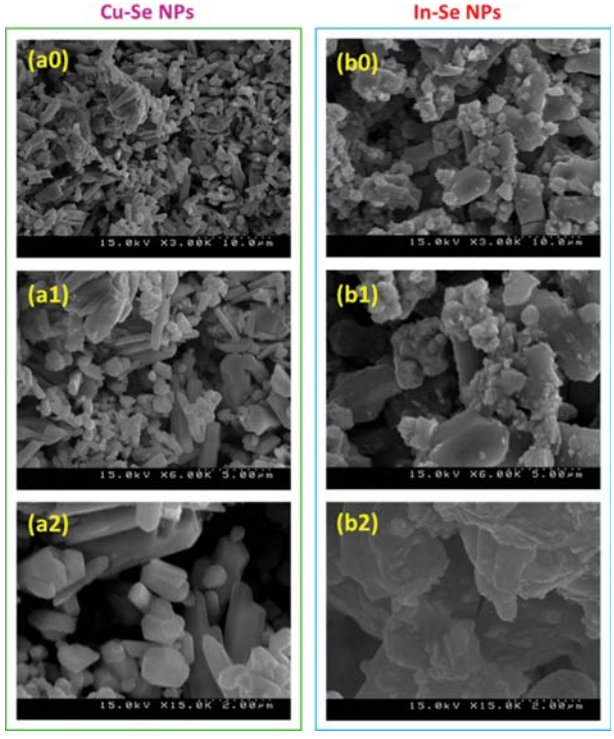

Fig. 5. SEM images of NG assisted binary NPs at different magnification.

1-4. FTIR Analysis

To confirm the NG capping and reaction paths of binary NPs, FTIR analysis was carried out and shown in Fig. 6. The FTIR spectrum of pure NG solution (Fig. 6(a)) shows peaks at 625 cm^{-1}, 1,363 cm^{-1}, 1,643 cm^{-1}, and 3,307 cm^{-1}. The polysaccharides contain functional groups such as CH_3, C=C, C-O, and C-N [31]. The broad peak centered at 625 cm^{-1} is due to C-C bonds, whereas a small bump observed at 1,363 cm^{-1} is due to C-O [31]. The peak at 1,643

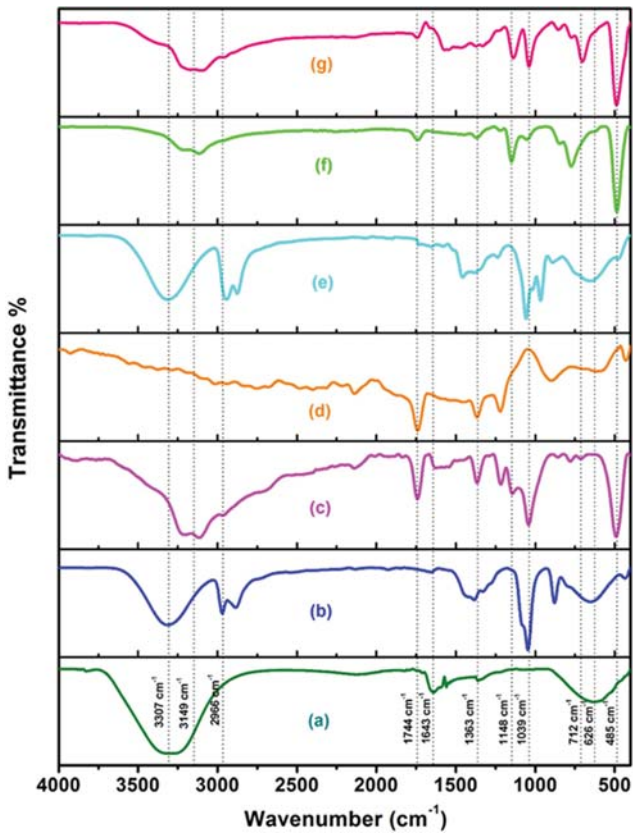

Fig. 6. FTIR spectra of as-prepared (a) NG-solution, (b) $CuCl_2$+ EtOH - solution, (c) Cu-Se NPs without NG, (d) Cu-Se NPs with NG, (e) $InCl_3$+IPA - solution, (f) In-Se NPs without NG, and (g) In-Se NPs with NG, respectively.

cm^{-1} is attributed to the asymmetric stretch of carboxylate groups (C=C). The broad peak centered at 3,307 cm^{-1} is due to the presence of OH-group vibrations [31,41]. The identified hydroxyl and carbonyl functional groups present in the NG were responsible for the reduction and stabilization of binary Cu-Se and In-Se NPs as described in the introduction. Table 1 represents a summary of the observed FTIR modes and their corresponding functional groups.

Further, a clear shifting in the peak positions can be seen between the FTIR spectra of precursor solutions and binary NPs with and without NG. Particularly, the FTIR modes observed in the wavenumber regions of 3,307-2,996 cm^{-1}, 1,744-1,643 cm^{-1}, 1,148-1,039 cm^{-1}, and 712-485 cm^{-1} are clearly shifted or altered when compared with FTIR spectra of precursor solutions to binary NPs with and without NG. The FTIR modes observed in the region of 3,307-2,996 cm^{-1} are due to OH-group vibrations [31,41]. The modes observed in the region of 1,744-1,643 cm^{-1} are due to -COOH and C=C functional groups [42]. The modes observed in the region of 1,148-1,039 cm^{-1} are due to the C-H and Se-C vibrations [42,43], whereas the modes observed in the region of 712-485 cm^{-1} are due to the C-C and metal-OH bounds [44,45]. A clear shifting of these peaks in the FTIR spectra of binary NPs with and without NG confirms the chemical reaction between the precursors and NG.

More interestingly, in the case of Cu-Se NPs without NG, the FTIR spectrum shows OH group stretching vibrations modes at 3,149 cm^{-1} (see Fig. 6(c)); however, this mode is not observed in the FTIR spectrum of Cu-Se NPs with NG. This indicates a clear capping/passivation of Cu-Se NPs by NG. Consequently, Cu-Se NPs were prevented from air oxidation. However, in the case of In-Se NPs, the FTIR spectrum of In-Se NPs with NG shows significant alteration as well as an intensity decrement in the vibrations modes of OH group. Therefore, it is confirmed that the use of NG is beneficial in the synthesis of binary NPs as reducing agent and capping agent. In addition, the capping action of NG prevents the binary NPs from oxidation as also evident from XRD and EDS analysis.

1-5. TG-DTA Analysis

To test the thermal stability and evaporation of the solvents, TG-DTA with simultaneous DSC was performed on the binary NPs and powder scrubbed from the Cu-In-Se precursor film in the temperature range of 50-600 °C and shown in Fig. 7. The as-synthesized NG assisted Cu-Se and In-Se NPs show three regions of weight loss at 65-115 °C, 140-185 °C, and 200-400 °C. The weight loss in the region of 65-115 °C is ascribed to endothermic evaporation of lower boiling point solvents such as MeOH, H_2O and ethylenediamine adsorbed on the surface of binary NPs. The weight loss in the region of 140-185 °C is due to the evaporation of slightly higher boiling point solvents such as ethylenediamine (b.p.=116 °C) and NG (b.p.=~120-150 °C). The weight loss in the region between 200 and 400 °C corresponds to the volatilization of excess 'Se' [46-49].

On the other hand, the powder scrubbed from the Cu-In-Se precursor films shows only two regions of weight loss in the range of 180-300 °C and 340-440 °C. It can be seen from Fig. 7 that a few peaks below 200 °C (those observed in the case of as-synthesized binary NPs) are suppressed. This may be due to the following reason: The precursor films were deposited at a temperature of 80 °C

Table 1. Summary of the observed FTIR modes and their corresponding functional groups

Specimen	FTIR modes (cm^{-1})	Possible functional groups	References
Pure NG solution	625	C-C	[31]
	1363	C-O	
	1643	C=C	
	3307	OH-group	
Binary NPs (Cu-Se and In-Se)	712-485	C-C and metal-OH bounds	[31,41-45]
	1148-1039	C-H and Se-C vibrations	
	1744-1643	-COOH and C=C groups	
	3307-2996	OH-group	

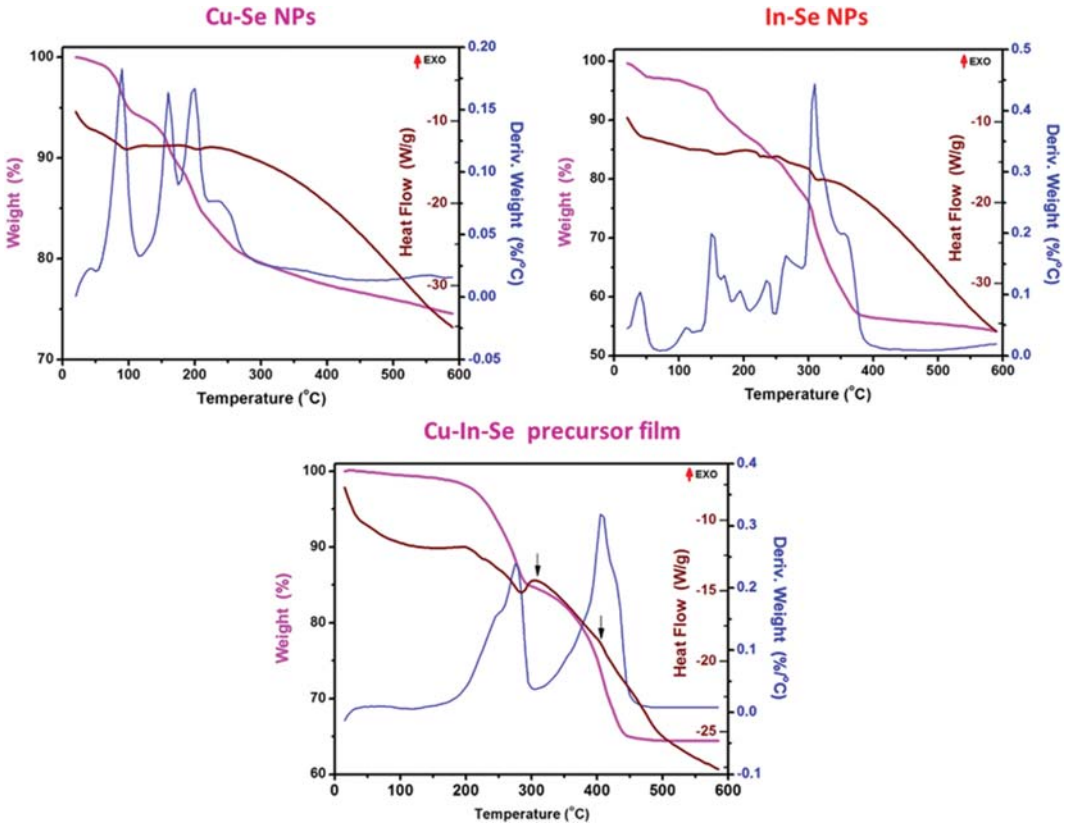

Fig. 7. TG-DTA curves of NG assisted Cu-Se and In-Se NPs and Cu-In-Se precursor film.

and allowed for drying at 120 °C for 5 min on a hot-plate. The coating and drying process led to the evaporation of lower boiling point solvents such as MeOH, H_2O, and ethylenediamine. Therefore, the characteristic peaks of these solvents were not found in the TG-DTA curves of the powder scrubbed from Cu-In-Se precursor films. Hence, only two regions of weight loss were observed in this case. The weight loss in the first region between 180 °C and 300 °C is attributed to the evaporation of slightly higher boiling point solvents such as ethylenediamine, MEA, and excess 'Se' [48]. The weight loss in the second region between 340 °C and 440 °C is ascribed to the melting of $CuSe_2$, CuSe, and volatilization of excess 'Se' [50-53]. Table 2 represents a summary of the observed TG-DTA peaks and species eliminated with temperature.

The peritectic decomposition of $CuSe_2$ to CuSe and a Se-rich liquid was evidenced by many studies at a temperature >345 °C [51,52]. It is reported that this liquid phase can assist the grain growth of $CuInSe_2$ [50]. Moreover, in the formation of CISe, the reactions between $CuSe+In_4Se_3$ and $CuSe_2+In_4Se_3$ are exothermic [50]. In our case also, a few peaks (see the arrow marks in Fig. 7) indicated the initiation of aforesaid reactions between $CuSe+In_4Se_3$ and $CuSe_2+In_4Se_3$ for >307 °C. Since the Cu-In-Se precursor film was a mixture of both NG assisted binary Cu-Se and In-Se NPs, the aforesaid reaction between CuSe, $CuSe_2$, and In_4Se_3 phases triggered the formation of CISe at a temperature >300 °C. Further, it can be observed in Fig. 7 that the weight loss after 450 °C is completely ceased. This indicates the complete evaporation of all solvents used in the synthesis of binary NPs as well as in the ink formation. Therefore, the Cu-In-Se precursor films were annealed at 500 °C for 20 min under N_2 to obtain the CISe absorber layers. As stated in the introduction section, the growth of single-phase CISe can proceed through the inter-diffusion of Cu and In between the Cu-Se, and In-Se [54].

2. Properties of CISe Absorber Layer

2-1. Structural Analysis

Fig. 8(a) shows the XRD patterns of the Cu-In-Se precursor and

Table 2. Summary of TG-DTA analysis

Specimen	Temperature range (°C)	Species eliminated	References
NG assisted Cu-Se and In-Se NPs	65-115	MeOH, H_2O, and ethylenediamine	[46-49]
	140-185	NG and MEA	
	200-400	Excess 'Se'	
Cu-In-Se precursor film	180-300	NG, MEA and excess 'Se'	[50-53]
	340-440	Excess 'Se', CuSe and $CuSe_2$	

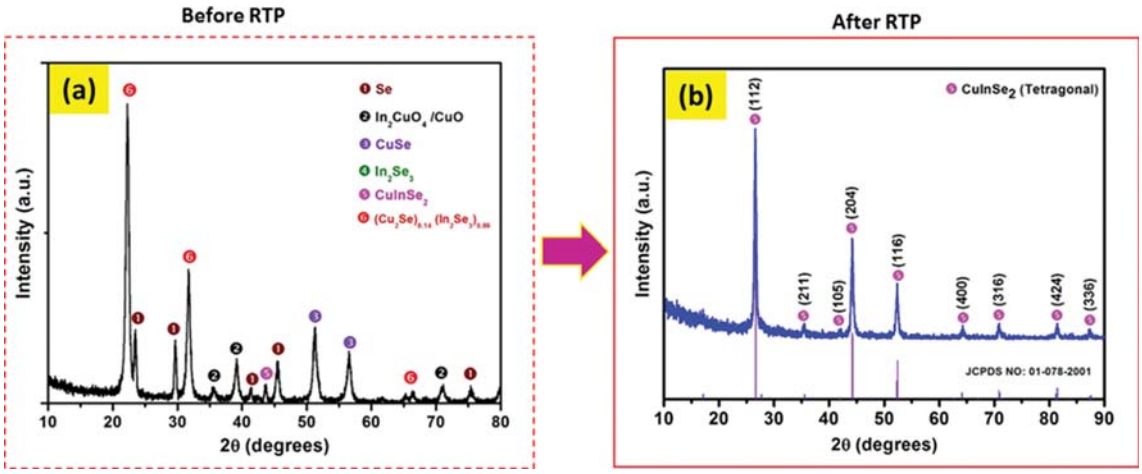

Fig. 8. XRD pattern of Cu-In-Se precursor film (before RTP) and CISe absorber layer (after RTP).

CISe absorber layer. The XRD pattern of Cu-In-Se precursor film (before RTP) showed multiple peaks related to Se, Cu_2Se, CuSe, In_2Se_3, oxides of Cu/In, and CISe phases (as per JCPDS-2004). It can be seen that the XRD pattern of Cu-In-Se precursor film is different from those of respective binary NPs. This is due to the recrystallization process over the substrate surface during the spray coating and drying process. As revealed by the XRD analysis, the formation of multi-phases of Cu-In-Se and CISe indicates the good dispersion and mixing of binary Cu-Se and In-Se NPs in i-BuOH : MEA solvent.

To obtain the CISe absorber layer, the Cu-In-Se precursor film was annealed by RTP. Fig. 8(b) shows the XRD pattern of CISe absorber layer after RTP. After RTP, the film shows the formation of single phase CISe with tetragonal structure. All the diffraction peaks were indexed to chalcopyrite tetragonal structure, which well matches with the standard JCPDS card No. 078-2001 as well as with the reported literature [53,55]. No impurity or secondary related phases were identified from the XRD analysis. The XRD pattern of CISe absorber layer (Fig. 8(b)) shows three major sharp and intense peaks at 2θ equal to 26.60°, 44.19°, and 52.37°, which are indexed to (112), (204)/(220), and (116)/(312) planes, respectively. In addition, a few minor intense peaks are also observed at 2θ equals to 35.43°, 41.89°, 64.29°, 70.82°, 81.38°, and 87.44°. These minor peaks were indexed to (211), (105)/(213), (008)/(400), (316)/(332), (228)/(424), and (336)/(512) planes, respectively. It is reported that the major peaks observed at 26.60°, 44.19°, and 52.37° are common to both sphalerite and chalcopyrite structures [55]. Therefore, to confirm the chalcopyrite structure, the presence of minor peaks corresponding to (101), (103), and (211) planes are necessary [55]. These minor peaks are observed at 17.12°, 27.68°, and 35.48°. In the present case also, the presence of minor (211) peak at 35.43° confirms the formation of chalcopyrite structure of CISe absorber layer.

To further confirm the phase purity of CISe absorber layer, Raman analysis was carried out. Fig. 9 shows the Raman spectrum of CISe absorber layer. A high intense mode at 173 cm^{-1} (with FWHM of 12 cm^{-1}) confirms the formation of chalcopyrite CISe phase. The peak at 173 cm^{-1} is attributed to the A_1 mode of CISe chalcopyrite tetragonal structure, which also agrees well with the reported literature [56]. In addition to A_1 mode, a feeble and broad bump centered at 215 cm^{-1} was also observed. This corresponded to the B_2 mode of CISe tetragonal structure [56]. Although the XRD pattern of CISe absorber layer shows single phase tetragonal CISe, a careful observation of the Raman spectrum indicates the presence of Cu_2Se [57] and $InSe_2$ [58] traces. The vertical dotted lines shown in Fig. 9 indicate the respective positions of Cu_2Se and $InSe_2$ phases. Usually, the presence of Cu_2Se phase would create shunt paths and poor p-n junction [59] at the device level. However, in the present case, the intensity of Cu_2Se phase mode is very low. Therefore, the effect of Cu_2Se phase on the device power conversion efficiency is expected to be less.

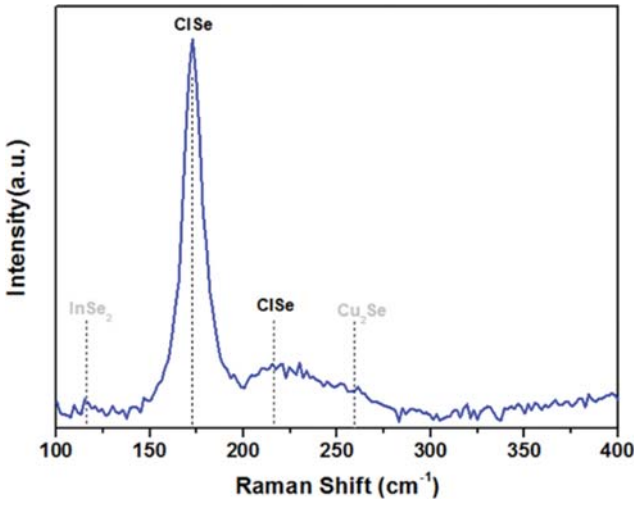

Fig. 9. Raman spectrum of CISe absorber layer.

2-2. Morphological Analysis

The morphology of CISe absorber layer was examined through SEM. Fig. 10 shows the planar and cross-sectional SEM images of CISe absorber layer before and after RTP. The thickness of the as-coated Cu-In-Se precursor film was ~3 μm. As can be seen from Fig. 10, the surface of the Cu-In-Se precursor layer before RTP shows

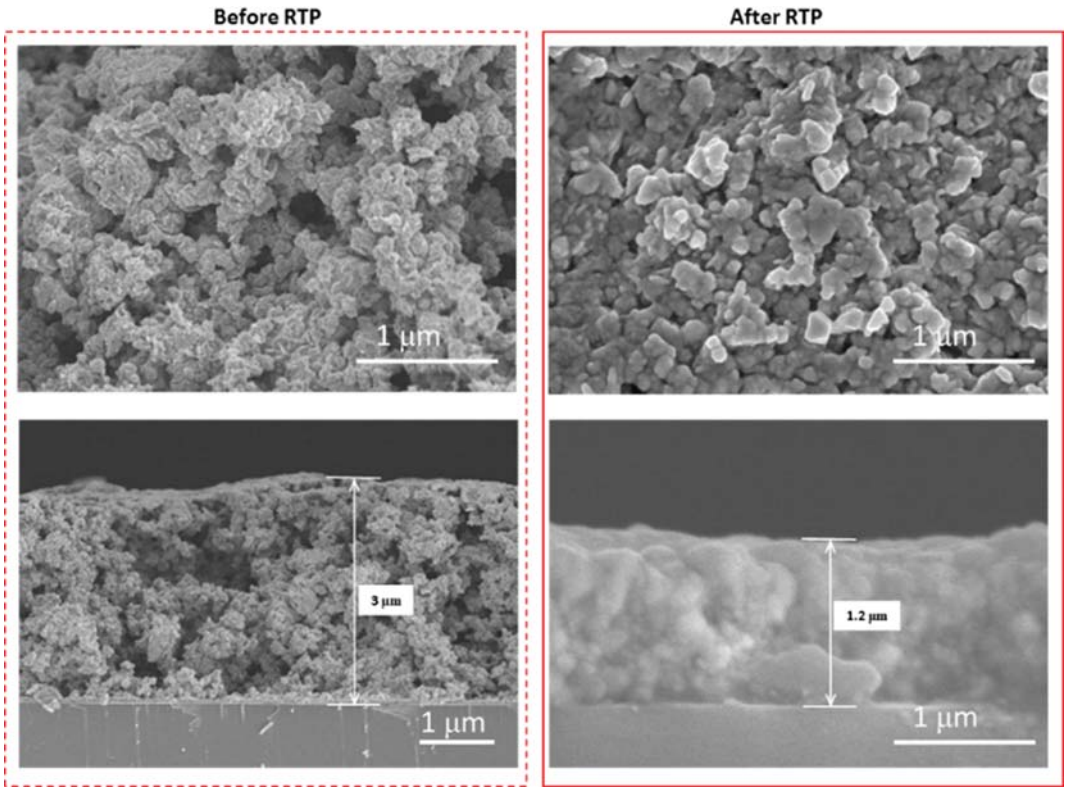

Fig. 10. SEM images of Cu-In-Se precursor film and CISe absorber layer on Mo: Planar (top) and cross-sectional (bottom).

small size grains with porosity. However, after RTP the grains grew bigger with compact morphology. The thickness of CISe absorber layer was reduced to ~1.2 μm owing to the evaporation of solvents. The EDS analysis of CISe absorber layer revealed an atomic ratio of 1.03 : 0.98 : 1.98 for Cu : In : Se. The measured atomic ratios of Cu : In : Se was found to be close to the standard stoichiometry of CISe (1 : 1 : 2). As can be seen from Fig. 10, even though the grain size of CISe absorber layer is considerably increased after RTP, the surface of CISe absorber layer shows some voids and non-uniform grain growth. However, the CISe absorber layer was found to be free from the cracks and delamination after coating, drying, and thermal treatments. This was due to the following reason. Since CISe absorber layer was deposited using the gum assisted binary NPs, it was free from the cracks and delamination. As discussed in the introduction section, the gum used in the synthesis acts as a natural binder in the coating process. Therefore, the films coated using NG assisted binary NPs are free from the cracks and delamination. Thus, in the present method, the use of organic binders are eliminated.

2-3. Optical Analysis

The CISe absorber layer was further analyzed by UV-Vis-NIR spectroscopy to examine its optical properties. A parallel prepared sample on bare soda lime glass was used for this measurement. The UV-Vis-NIR absorption spectrum was measured in the wavelength range of 400-1,600 nm and shown in Fig. 11.

The UV-Vis-NIR spectrum of CISe absorber layer shows clear absorption edge at a cut-off wavelength of 1,236 nm. The optical band gap energy of the CISe absorber layer was estimated using a simple relation, $E_g = h \times c/\lambda$ (h is Planck's constant, c is the speed of light, and λ is the absorption cut-off wavelength). Using this relation, the band gap energy of CISe absorber layer was estimated, which is equals to 0.99 eV. A slight decrease in the band gap energy of the present film compared to the reported value of CISe (1.02 eV) [60] was due to the stoichiometric deviation. A slight deviation from the standard stoichiometry was due to the evaporation of lower melting point 'In' and 'Se' atoms from the CISe absorber layer during the rapid thermal annealing process [61].

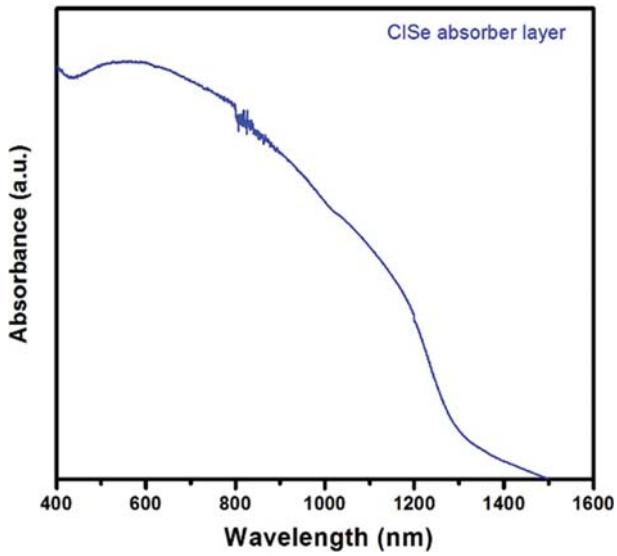

Fig. 11. UV-Vis-NIR absorption spectrum of CISe absorber layer.

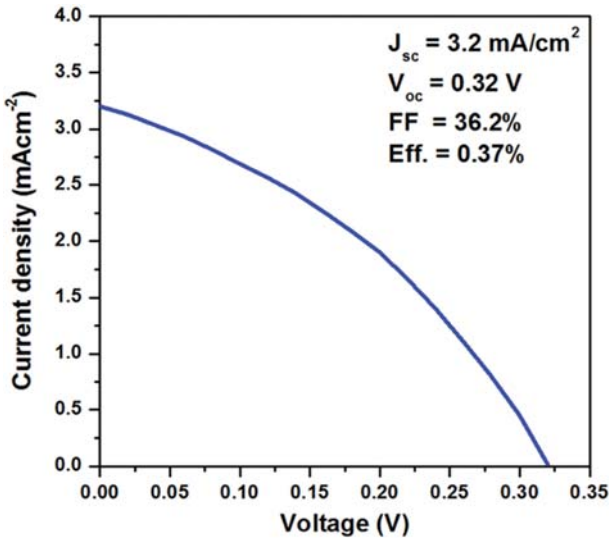

Fig. 12. The light illuminated J-V characteristic of the CISe absorber layer.

3. Device Characteristics

The CISe absorber layer was integrated into a photovoltaic device with a device architecture of SLG/Mo/CIS/CdS/i-ZnO/Al : ZnO/Ni/Ag. The antireflection layer was illuminated not performed for the devices tested in this study. Fig. 12 shows the current density-voltage (J-V) characteristics of the fabricated CISe NPs device. Despite the slightly Cu-rich composition (Cu/In=1.03) and lower band gap (0.99 eV), the fabricated solar cells show a maximum power conversion efficiency of 0.37% with an open circuit voltage (V_{OC}), short circuit current density (J_{SC}), and fill factor (FF) of 0.32 V, 3.2 mA cm^{-2} and 36.2%, respectively.

The main reason for low PCE of the present device is due to the copper-rich composition of CISe absorber layer. As presumed in the Raman analysis, the segregation of conductive Cu-rich binary phase such as Cu_2Se created the shunt paths in the absorber layer, which played a detrimental role on device efficiency [59]. As evidenced by Raman analysis, the detected trace amount of Cu_2Se phase in the CISe absorber layer also supports this assumption. In addition, the observed lower V_{OC} is another reason for the lower PCE. The obtained lower V_{OC} was attributed to low grain size and band gap energy of the present CISe absorber layer. Further, it can be seen from Fig. 10 that the CISe absorber layer has less compactness with small grains. It is reported that these small grains can produce a larger number of grain boundaries [37,62]. Therefore, they act as trapping centers to the light-generated minority carries. Consequently, the fabricated CISe NPs solar cell show low PCE.

To improve the power conversion efficiency, additional steps such as (i) KCN etching for removal of the Cu-rich binary phases, (ii) supply of 'Se' vapor is helpful to compensate the loss of 'Se' and porosity of the absorber layer after annealing, (iii) doping with gallium will be helpful to widen the band gap of CISe [63], (iv) treating with NaCl-$InCl_3$ flux can improve the grain size and removal of Cu-rich binary phases in the CISe absorber layer [49], and (v) optimization of the post thermal treatment of the CISe absorber layer is desired to improve the grain size and compactness [62]. Those experiments are underway.

On the other hand, carbon contamination is also another big issue in the nanoparticle based solar cells. In the present case, a small amount of carbon was observed in the films possibly due to the adsorbed functional groups of gum on the NPs. Since no external binders were used in the present case, only a small amount of carbon residues should be present in the films. The residues of carbon can restrict the grain growth of the absorber layer. Therefore, this may be one of the reasons for the obtained lower PCE. However, there are controversial statements on the carbon content in the literature [64,65]. Rehan et al. [66] reported that a certain amount of carbon contamination in CISe absorber shows a beneficial impact on PCE.

In this regard, the gum assisted binary NPs synthesis and their utilization in the preparation of CISe absorber layer is quite beneficial to lower the manufacturing cost of CISe thin film solar cells. As no external binders were used, the possibility of carbon residues in the films was reduced to a greater extent. In addition, the present strategy followed herein is also useful to reduce the risks encountered due to the use of toxic organic solvents and binders. Therefore, we hope that the present method is unique and opens new path for the production of eco-friendly CISe thin film solar cells.

CONCLUSIONS

Se-rich binary Cu-Se and In-Se NPs were prepared by a simple, green, and cost-effective method using gum exudates from a cherry blossom tree. As the necessary emulsification was provided by the NG used in the reaction, no additional binder/additive was used to deposit the Cu-In-Se precursor film. After RTP, the XRD analysis showed single phase CISe with tetragonal chalcopyrite structure. However, Raman analysis showed a trace amount of Cu_2Se due to little evaporation of lower melting point 'In' and 'Se' atoms. Optical analysis showed a band gap energy of 0.99 eV to CISe absorber layer. The fabricated CISe NPs devices showed an efficiency of 0.37%. The analysis showed that the stoichiometric deviation, incorporation of Cu_2Se phase, and non-uniform grain growth mitigated the PCE of the present devices. Optimization of CISe absorber layer along with some additional treatments will definitely improve the efficiency. This study shows the potential of NG assisted binary NPs use in the fabrication of low-cost and eco-friendly thin film solar cells.

CONFLICT OF INTEREST

There are no conflicts of interest to declare.

ACKNOWLEDGEMENTS

This work was supported by the 2017 Yeungnam University research grant and by "The Human Resources Program in Energy Technology" of the Korea Institute of Energy Technology Evaluation and Planning (KETEP), granted financial resource from the Ministry of Trade, Industry & Energy, the Republic of Korea (No.

20154030200760).

REFERENCES

1. E. Jiaqiang, M. Pham, Y. Deng, T. Nguyen, D. VinhNguyen, D. Le, Z. Wei, P. Qingguo and Z. Zhiqing, *Energy*, **149**, 979 (2018).
2. Z. Zhang, E. Jiaqiang, Y. Deng, M. Pham, W. Zuo, P. Qingguo and Y. Zibin, *Energy Convers. Manag.*, **159**, 244 (2018).
3. A. Rockett and R. W. Birkmire, *J. Appl. Phys.*, **70**, R81 (1991).
4. O. Lundberg, M. Edoff and L. Stolt, *Thin Solid Films*, **480-481**, 520 (2005).
5. T. Dullweber, G. Hanna, W. Shams-Kolahi, A. Schwartzlander, M. A. Contreras, R. Noufi and H. W. Schock, *Thin Solid Films*, **361**, 478 (2000).
6. L. L. Kazmerski, F. R. White and G. K. Morgan, *Appl. Phys. Lett.*, **29**, 268 (1976).
7. P. Jackson, R. Wuerz, D. Hariskos, E. Lotter, W. Witte and M. Powalla, *Phys. Status Solidi - Rapid Res. Lett.*, **10**, 583 (2016).
8. W. Wang, Y. W. Su and C. H. Chang, *Sol. Energy Mater. Sol. Cells*, **95**, 2616 (2011).
9. M. A. Malik, N. Revaprasadu and K. Ramasamy, Nanomaterials for solar energy conversion (2013).
10. Q. Guo, G. M. Ford, H. W. Hillhouse and R. Agrawal, *Nano Lett.*, **9**, 3060 (2009).
11. G. M. Hanket, R. W. Birkmire, S. C. Jackson and R. E. Rocheleau, Roll-to-roll deposition of a semiconductor film on a flexible substrate for photovoltaics: Conception to reality (2009).
12. J. Luo, S. D. Tilley, L. Steier, M. Schreier, M. T. Mayer, H. J. Fan and M. Grätzel, *Nano Lett.*, **15**, 1395 (2015).
13. D. Zhao, Q. Tian, Z. Zhou, G. Wang, Y. Meng, D. Kou, W. Zhou and S. Wu, *J. Mater. Chem. A Mater. Energy Sustain.*, **3**, 19263 (2015).
14. G. Wang, S. Wang, Y. Cui and D. Pan, *Chem. Mater.*, **24**, 3993 (2012).
15. P. Y. Lin and Y. S. Fu, *Mater. Lett.*, **75**, 65 (2012).
16. S. Jeong, B.-S. Lee, S. Ahn, K. Yoon, Y.-H. Seo, Y. Choi and B.-H. Ryu, *Energy Environ. Sci.*, **5**, 7539 (2012).
17. S. K. S. Ahn, Y. J. Choi, K. Kim, Y. J. Eo, A. Cho, J. Gwak, J. H. Yun, K. Shin, S. K. S. Ahn and K. Yoon, *ChemSusChem*, **6**, 1282 (2013).
18. A. Cho, S. Ahn, J. H. Yun, Y. J. Eo, H. Song and K. Yoon, *Sol. Energy Mater. Sol. Cells*, **110**, 126 (2013).
19. A. Cho, S. Ahn, J. Ho Yun, J. Gwak, S. Kyu Ahn, K. Shin, H. Song and K. Hoon Yoon, *Sol. Energy Mater. Sol. Cells*, **109**, 17 (2013).
20. B.-S. Lee, Y. Hwang, H. N. Pham, J. Y. Kim, M. H. Song and D.-K. Lee, *J. Mater. Chem. A*, **3**, 15889 (2015).
21. J. Maes, R. Dierick, B. Capon, C. Detavernier and Z. Hens, *Sol. Energy Mater. Sol. Cells*, **145**, 126 (2016).
22. N. S. Kozhevnikova, A. S. Vorokh, O. I. Gyrdasova, I. V. Baklanova, A. N. Titov and M. V. Kuznetsov, *Nanosyst. Physics, Chem. Math.*, **8**, 787 (2017).
23. H. Lee, D. Jeong, T. Mun, B. Pejjai, V. R. M. Reddy, T. J. Anderson and C. Park, *Korean J. Chem. Eng.*, **33**, 2486 (2016).
24. F. Liu, J. Zhu, Y. Xu, L. Zhou and S. Dai, *Nanoscale*, **8**, 10021 (2016).
25. E. Dilena, Y. Xie, R. Brescia, M. Prato, L. Maserati, R. Krahne, A. Paolella, G. Bertoni, M. Povia, I. Moreels and L. Manna, *Chem. Mater.*, **25**, 3180 (2013).
26. W. Wang, S.-Y. Han, S.-J. Sung, D.-H. Kim and C.-H. Chang, *Phys. Chem. Chem. Phys.*, **14**, 11154 (2012).
27. S. Ahmed and S. Ikram, *Nano Res. Appl.*, **1**, 1 (2015).
28. M. Venkatesham, D. Ayodhya, A. Madhusudhan, A. Santoshi Kumari, G. Veerabhadram and K. Girija Mangatayaru, *J. Clust. Sci.*, **25**, 409 (2014).
29. S. Hedayati and M. Niakousari, *J. Food Process. Preserv.*, **39**, 2001 (2015).
30. P. S. Gils, D. Ray and P. K. Sahoo, *Int. J. Biol. Macromol.*, **46**, 237 (2010).
31. R. M. A. Daoub, A. H. Elmubarak, M. Misran, E. A. Hassan and M. E. Osman, *J. Saudi Soc. Agric. Sci.*, **17**, 241 (2018), DOI:10.1016/j.jssas.2016.05.002
32. A. H. Cheshme Khavar, A. R. Mahjoub, F. Tajabadi, M. Dehghani and N. Taghavinia, *Eur. J. Inorg. Chem.*, **2015**, 5793 (2015).
33. G. Chen, W. Liu, G. Jiang, J. Li and C. Zhu, *J. Alloys Compd.*, **531**, 91 (2012).
34. T. Todorov and D. B. Mitz, *Eur. J. Inorg. Chem.*, **2010**, 17 (2010), DOI:10.1002/ejic.200900837.
35. B. Pejjai, V. Reddy, M. Reddy, S. Gedi and C. Park, *J. Ind. Eng. Chem.*, **60**, 19 (2018).
36. B. Pejjai, V. R. Minnam Reddy, S. Gedi and C. Park, *Int. J. Hydrogen Energy*, **42**, 2790 (2017).
37. B. Pejjai, V. R. Minnam Reddy, K. Seku, M. R. Pallavolu and C. Park, *New J. Chem.*, **42**, 4843 (2018).
38. M. Outokesh, M. Hosseinpour, S. J. Ahmadi, T. Mousavand, S. Sadjadi and W. Soltanian, *Ind. Eng. Chem. Res.*, **50**, 3540 (2011).
39. K. Nose, Y. Soma, T. Omata and S. Otsuka-Yao-Matsuo, *Chem. Mater.*, **21**, 2607 (2009).
40. H. Miyake, H. Ohtake and K. Sugiyama, *J. Cryst. Growth*, **156**, 404 (1995).
41. S. M. Hosseinpour-Mashkani, M. Salavati-Niasari and F. Mohandes, *J. Ind. Eng. Chem.*, **20**, 3800 (2014).
42. J. Ram Kumar, S. Ananthakumar and S. Moorthy Babu, *J. Electron. Mater.*, **46**, 296 (2017).
43. A. Permadi, M. Z. Fahmi, J.-K. Chen, J.-Y. Chang, C.-Y. Cheng, G.-Q. Wang and K.-L. Ou, *RSC Adv.*, **2**, 6018 (2012).
44. A. Goudarzi, A. D. Namghi and C.-S. Ha, *RSC Adv.*, **4**, 59764 (2014).
45. A. D. Sivagami, B. Sarma and A. Sarma, *Jpn. J. Appl. Phys.*, **55**, 01AE07 (2016).
46. B. P. Rand, J. Genoe, P. Heremans, J. Poortmans, A. R. Uhl, C. Fella, A. Chirilă, M. R. Kaelin, L. Karvonen, A. Weidenkaff, C. N. Borca, D. Grolimund, Y. E. Romanyuk, A. N. Tiwari, B. P. Rand, J. Genoe, P. Heremans and J. Poortmans, *Prog. Photovolt Res. Appl.*, **15**, 526 (2007).
47. A. R. Uhl, P. Fuchs, A. Rieger, F. Pianezzi, C. M. Sutter-Fella, L. Kranz, D. Keller, H. Hagendorfer, Y. E. Romanyuk, F. LaMattina, S. Yoon, L. Karvonen, T. M. Friedlmeier, E. Ahlswede, D. Van Genechten, F. Stassin, A. N. Tiwari, B. P. Rand, J. Genoe, P. Heremans and J. Poortmans, *Prog. Photovolt Res. Appl.*, **23**, 1110 (2015).
48. W. Liu, D. B. Mitzi, M. Yuan, A. J. Kellock, S. Jay Chey and O. Gunawan, *Chem. Mater.*, **22**, 1010 (2010).
49. M. Kurihara, F. Hayashi, K. Shimizu, H. Wagata, T. Hirano, Y. Nakajima, K. Yubuta, S. Oishi and K. Teshima, *Cryst. Growth Des.*, **16**, 1195 (2016).
50. E. Yassitepe, W. N. Shafarman and S. I. Shah, *J. Solid State Chem.*,

213, 198 (2014).
51. A. E. Zaghi, M. Buffiere, J. Koo, G. Brammertz, M. Batuk, C. Verbist, J. Hadermann, W. K. Kim, M. Meuris, J. Poortmans and J. Vleugels, *Thin Solid Films*, **582**, 11 (2015).
52. G. P. Bernardini and A. Catani, *Miner. Depos.*, **3**, 375 (1968).
53. J. B. Shim, C. G. Kim, D. J. Jeon, T. M. Chung, K. S. An, S. S. Lee, J. S. Lim, S. J. Jeong, B. K. Park and Y. K. Lee, *J. Phys. Chem. Solids*, **74**, 867 (2013).
54. S. T. Connor, C.-M. Hsu, B. D. Weil, S. Aloni and Y. Cui, *J. Am. Chem. Soc.*, **131**, 4962 (2009).
55. Q. Guo, S. J. Kim, M. Kar, W. N. Shafarman, R. W. Birkmire, E. A. Stach, R. Agrawal and H. W. Hillhouse, *Nano Lett.*, **8**, 2982 (2008).
56. Z. Han, D. Zhang, Q. Chen, T. Mei and S. Zhuang, *Powder Technol.*, **249**, 119 (2013).
57. J. H. Park, I. S. Yang and H. Y. Cho, *Appl. Phys. A*, **58**, 125 (1994).
58. J. Weszka, P. Daniel, A. Burian, A. M. Burian and A. T. Nguyen, *J. Non. Cryst. Solids*, **265**, 98 (2000).
59. Y. S. Lim, J. Jeong, J. Y. Kim, M. J. Ko, H. Kim, B. Kim, U. Jeong and D. Lee, *Sci. Technol.*, **117**, 11930 (2013).
60. Q. Chen, X. Dou, Z. Li, S. Cheng and S. Zhuang, *J. Phys. D. Appl. Phys.*, **44**, 455401 (2011).
61. J. E. Lee, H. Lee, D. Jeong, B. Pejjai, V. R. Minnam Reddy and C. Park, *Chinese J. Phys.*, **56**, 392 (2018), DOI:10.1016/j.cjph.2017.08.033
62. J. Y. Lee, S. O. Ryu and T. J. Lee, *Mol. Cryst. Liq. Cryst.*, **564**, 147 (2012).
63. F. Roux, S. Amtablian, M. Anton, G. Besnard, L. Bilhaut, P. Bommersbach, J. Braillon, C. Cayron, A. Disdier, H. Fournier, J. Garnier, A. Jannaud, J. Jouhannaud, A. Kaminski, N. Karst, S. Noël, S. Perraud, O. Poncelet, O. Raccurt, D. Rapisarda, A. Ricaud, D. Rouchon, M. Roumanie, E. Rouviere, O. Sicardy, F. Sonier, K. Tarasov, F. Tardif, M. Tomassini, J. Villanova, S. Noel, S. Perraud, O. Poncelet, O. Raccurt, D. Rapisarda, A. Ricaud, D. Rouchon, M. Roumanie, E. Rouviere, O. Sicardy, F. Sonier, K. Tarasov, F. Tardif, M. Tomassini and J. Villanova, *Sol. Energy Mater. Sol. Cells*, **115**, 86 (2013).
64. M. Buffiere, A. E. Zaghi, N. Lenaers, M. Batuk, S. Khelifi, J. Drijkoningen, J. Hamon, A. Stesmans, J. Kepa, V. V. Afanasev, J. Hadermann, J. DHaen, J. Manca, J. Vleugels, M. Meuris and J. Poortmans, *J. Phys. Chem. C*, **118**, 27201 (2014).
65. C. J. Hibberd, E. Chassaing, W. Liu, D. B. Mitzi, D. Lincot and A. N. Tiwari, *Prog. Photovoltaics Res. Appl.*, **18**, 434 (2010).
66. S. Rehan, K. Y. Kim, J. Han, Y. J. Eo, J. Gwak, S. K. Ahn, J. H. Yun, K. Yoon, A. Cho and S. Ahn, *ACS Appl. Mater. Interfaces*, **8**, 5261 (2016).